

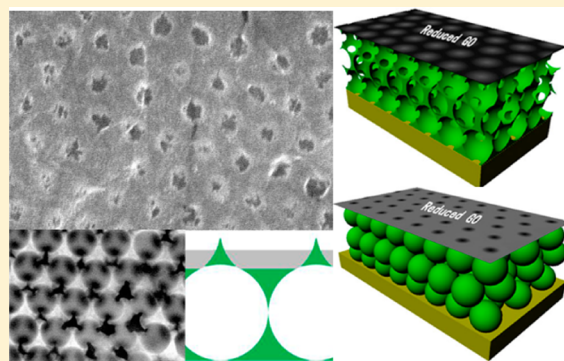
Patterning of Graphene via an In Situ Electrochemical Method using Ni Opal or Inverse-Opal Structures

Yuqiong Zhao, Ming Fu,* Yongna Zhang, Dawei He, and Yongsheng Wang

Key Laboratory of Luminescence and Optical Information, Ministry of Education, Institute of Optoelectronic Technology, Beijing Jiaotong University, Beijing 100044, People's Republic of China

S Supporting Information

ABSTRACT: The development of advanced methods for graphene with nanoscale width and periodic geometries is important to graphene-based electronic and optical devices. Metal inverse opals and opals were used as reliable nanopatterned electrodes for the electrochemical reactions of graphene oxide (GO) films at -0.8 to -1.5 V versus saturated calomel electrode. Graphene with redox patterns was formed by limited reduction time. Reduced GO (RGO) films with deeper surface impress patterns were formed after electrochemical reductions and varied according to the surface geometries of the Ni inverse opals. The resistivity of the RGO using Ni solid films and inverse opals decreased rapidly because a connected RGO formed at the beginning of the reduction. In contrast, the resistivity of RGO reduced by Ni opals did not show a significant decrease in the beginning because of the disconnected reduction. The formed periodic undulations of RGO structures did not show the coupling of optical wavelength, but shifted the stop band of colloidal crystals covered under them.



INTRODUCTION

Graphene has emerged as an exciting material with great potential affecting many areas of technology such as touch screen,¹ E-paper,² foldable organic light-emitting diode,³ high-frequency transistor,⁴ solid-state mode-locked laser,⁵ photodetector,⁶ polarization controller,⁷ optical modulator,⁸ and energy storages^{9,10} because it possesses many outstanding properties in strength,¹¹ electrical and thermal conductivity,¹² high optical transmittance,¹³ tunable surface conductivity by doping¹⁴ or applying an external transverse electric field,¹⁵ high optical nonlinearity,¹⁶ and giant Faraday effect.¹⁷ However, the zero-band gap nature¹⁸ of graphene limits its applications to electronic and optoelectronic devices. The band gap of graphene can be generated or modified using different methods such as the formation of nanoribbons or nanomeshes,^{19,20} doping,¹⁴ and breaking symmetry in bilayer graphene.²¹

As graphene nanostructures with feature sizes <10 nm possess necessary band gaps for optoelectronic applications,^{22–24} many patterning methods have been developed providing graphene with a nanoscale width such as photomask-assisted photocatalysis,^{25,26} surface template-assisted anisotropic etching,^{27–29} template-assisted chemical decoration,^{30,31} and direct laser etching.³² Among these methods, monolayer colloidal spheres have been proven as reliable two-dimensional (2D) masks. However, the 2D masks only played the roles of geometric shading or photocatalysis in the current methods. The usage of the electric conductivity of the masks in graphene patterning has not been developed yet. If the masks can serve as electron channels for graphene patterning, not only 2D

structures, but also different surfaces of three-dimensional (3D) structures can be applied to the graphene patterning process.

Because electrochemical reduction is one of the successful methods in the synthesis of graphene from graphene oxide (GO),^{9,10,33–41} reduction in localized nanoareas can be achieved near the contact points between GO and the used patterning structure. The in situ electrochemistry method is advantageous in controlling both the redox locations and quantity of reduction electrons during the patterned reduction process of GO.

In this study, we developed an electrochemical patterning method of graphene using the surface of metallic inverse-opal and opal structures. Patterned graphene can be formed by the in situ reduction method using GO. In this manner, graphene with different redox status patterns and geometrical impresses were obtained. The periodic morphologies, redox status, and electronic and optical properties were investigated.

EXPERIMENTAL SECTION

3D Ni inverse-opal or opal structures were used as the mask of the nanopatterning of GO by an electrochemical route as shown in Figure 1. Ni inverse opals were formed by colloidal crystal template-assisted electrodeposition, and Ni opals were obtained by the double replication through ZnO inverse opals.

Received: July 21, 2014

Revised: September 2, 2014

Published: September 4, 2014



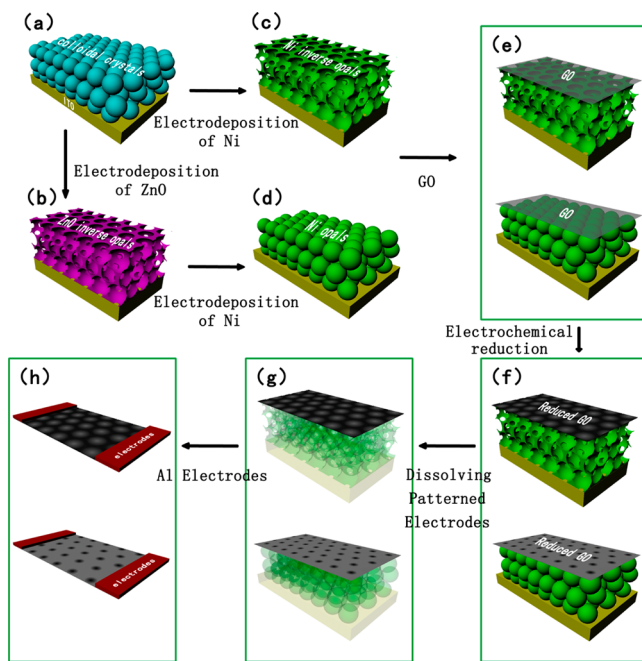


Figure 1. Scheme for the in situ electrochemical reduction of graphene using Ni inverse opals and opals. (a) Self-assembled colloidal crystals were used as the templates for the formation of (b) ZnO inverse opals, (c) Ni inverse opals, and (d) Ni opal structures by electrodeposition. (e, f) In situ reduction of the network or dotted patterns in GO were performed using Ni inverse opals or opals. (g, h) The electric conductivity of RGO was tested after Ni was removed.

The colloidal crystal template arrays were formed by the self-assembly of monodispersed polystyrene colloidal crystal microspheres with diameter of 265 nm onto indium tin oxide (ITO) substrates at 55 °C and 30% relative humidity. CHI660A/D/E electrochemical workstations were used for the fabrication of Ni inverse opals, ZnO inverse opals, and Ni opals.

The colloidal crystal-covered ITO substrates were used as the working electrodes for Ni electroplating. The electrodeposition experiments were performed by the galvanostatic method in a

current density of 0.001 A/cm² for 1 min in a Ni plating solution (2.13 M NiSO₄, 0.35 M NiCl₂, and 0.43 M H₃BO₃) at room temperature. Then, Ni inverse-opal structures were obtained after the colloidal templates were dissolved in a toluene solution, as shown in Figure 1c.

The colloidal crystal-covered ITO substrates were used as the electrodeposition working electrode, while a saturated calomel electrode (SCE) was used as the reference electrode. The ZnO inverse-opal structures (Figure 1b) were electrodeposited by the potentiostatic method at the potential of -1 V for 1 h in a zinc nitrate solution (0.1 M) at 70 °C, followed by calcination at 450 °C for 1 h to obtain the ZnO inverse-opal structures. The Ni was electrochemically infiltrated into the interstices of the ZnO inverse-opal structures using the Ni plating process (same as the formation of Ni inverse-opal structures), while the ZnO inverse-opal structures were used as the electrodeposition working electrode. After the ZnO inverse-opal structures were dissolved in a 1 M NaOH solution for 36 h, the Ni opal structures were obtained as shown in Figure 1d.

The GO (diameter 1–5 μm, thickness 0.8–1.2 nm, Nanjing XFNANO Materials Tech Co., Nanjing, China) was added to water to make a suspension (0.1 wt %). The GO suspension with a volume of 22 μL/cm² was dropped onto the Ni opal/inverse-opal structures, affording the GO film after drying (Figure 1e).

In the subsequent patterning process, Ni structures were directly used as the patterned electronic channels for the reduction of the GO films covered on them. The patterning reduction of GO was performed in a saturated potassium chloride solution. The GO-covered Ni was used as the working electrode, while SCE was used as the reference electrode. The GO films were reduced by the potentiostatic method at the potential from -0.8 to -1.5 V for 10 s to 24 h at room temperature.

The Ni microstructures were dissolved in a 1 M HCl solution for 24–48 h (Figure 1g). After the patterning, the reduced GO (RGO) was transferred to a glass slide by removing Ni, and the electric conductivity was measured by current–voltage (I–V) test. Two aluminum electrodes with 150 μm gap were deposited on the GO film (Figure 1h). The I–V of the

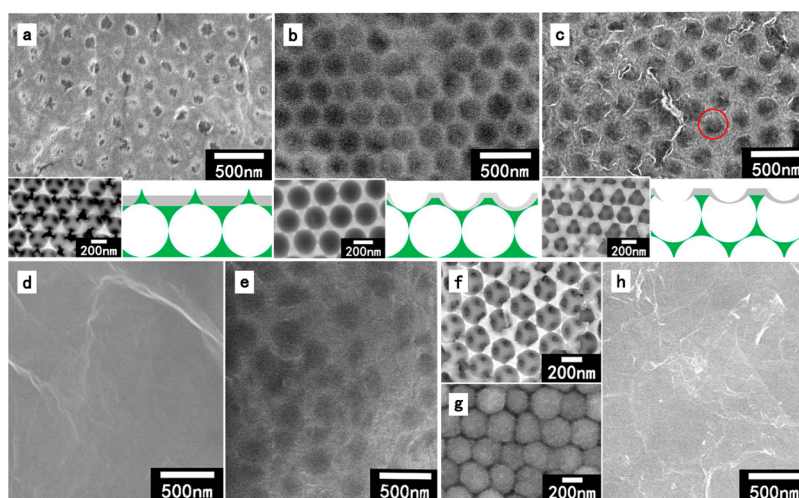


Figure 2. (a–c) SEM images of RGO fabricated using Ni inverse opals with different morphological surfaces shown in the insets of a–c. (d, e) SEM images of GO fabricated using inverse opals before the reduction showing (d) a smooth surface and (e) an inconspicuous pattern. (g) Ni opals via a double-template method using (f) ZnO inverse opals. (h) RGO produced using Ni opals.

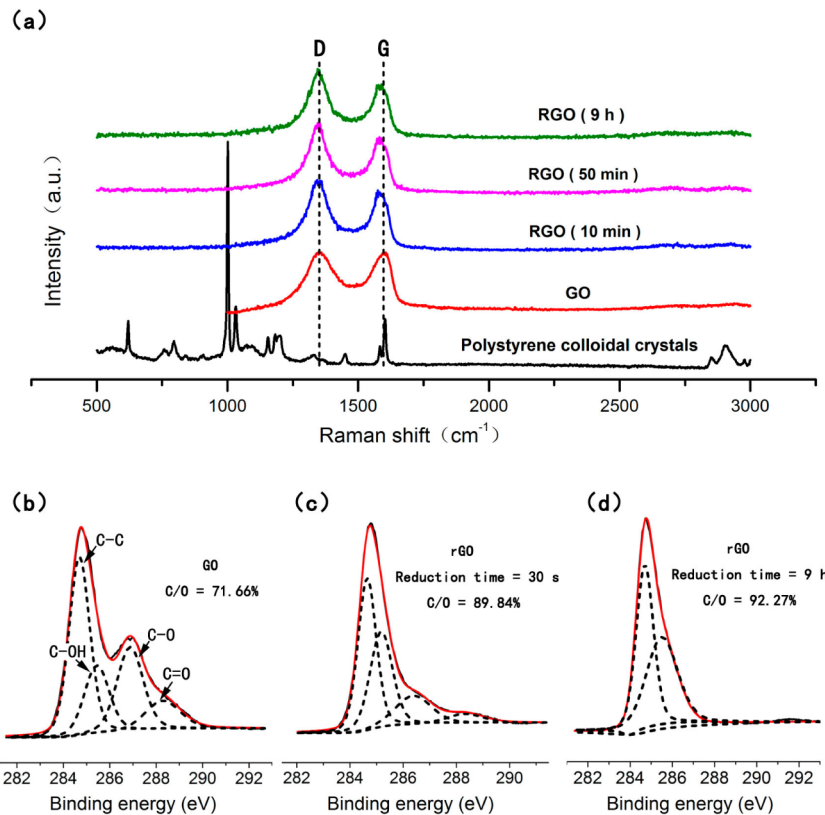


Figure 3. (a) Raman spectra of GO without reduction, RGO with different reduction times (from 10 min to 9 h) at -0.8 V using Ni inverse opals, and polystyrene colloidal crystals. (b–d) C 1s XPS spectra of (b) GO sample and (c) rGO sample reduced for 30 s, and for (d) 9 h.

patterning RGO was characterized using a Keithley 4200-SCS parameter analyzer together with a probe station.

The morphologies of Ni structures, GO, and RGO patterns were characterized using a scanning electron microscope (SEM, Hitachi 4800). The reflection spectra of RGO with periodic surface undulations and RGO on polystyrene opals were characterized using a silicon photodetector DSi200 equipped with a halogen lamp, Y-type fiber, monochromator, optical chopper, and lock-in amplifier (SR830). The optical simulations were carried out using the FDTD Solution software.

RESULTS AND DISCUSSIONS

Because different surface patterns of Ni were used in this study, GO would follow different impress and reduction patterns. The darker color shown in Figure 1f,g indicates the initial reduced areas of GO; the gray color indicates the unreduced areas. The initial network/dotted redox patterns of graphene would be produced on Ni inverse-opal and opal surfaces. Ni inverse opals fabricated using colloidal crystals by microspheres with a diameter of 265 nm were used as the electrodes for the localized in situ electrochemical reduction of GO. The inverse-opal structures formed by the colloidal crystal template arrays can theoretically produce contact surfaces with a much smaller neck width than their periodic dimensions, which made inverse opals the ideal electrodes for making patterned graphene with a nanoscale width.³¹ The inverse opals with a possible minimum contact width of ~ 11 nm fabricated using colloidal spheres with diameters of 265 nm are shown in the SEM image of Figure s1.

After the reduction of GO films (~ 110 nm in thickness by profilometer and density calculation), patterned RGO films

were formed. Figure 2a–c shows three typical SEM images of the RGO patterns after the electrochemical reduction process. Compared to the unpatterned GO reduced using solid Ni films (Figure s2), the GO surfaces formed via Ni inverse opals contain periodic imprint patterns. Because the thickness of the Ni electrodeposition changed slightly on the same sample, the top surfaces of Ni inverse opals had a different geometrical relationship between the positions of the removed colloidal template. Ni inverse-opal structures with several types of surface morphologies are shown in the insets of Figure 2a–c. Sharp prominences were formed when the top Ni surface was deposited on approximately half the thickness of colloidal spheres (Figure 2a, inset). Therefore, the resulting RGO showed related hexagonal holes from the surface view (Figure 2a). The resulting RGO shown in Figure 2b was formed using the Ni inverse-opal surface shown in Figure 2b, inset (Ni was slightly thicker than one of the colloidal layers). In this case, the RGO layer will possess the wrinkled surfaces of Ni inverse opals. When the Ni inverse-opal structure deposited was slightly thinner than one colloidal layer (Figure 2c, inset), the RGO layer formed depression holes in the cavity positions in inverse opals. The RGO films at the centers of periodic surface patterns were thinner or even empty (shown in red circle) because of the void nature of inverse opals. Although the RGO shows distinct imprint patterns (Figure 2a–c), the unreduced GO films fabricated after the dissolution of Ni only showed unpatterned (smooth) surfaces (Figure 2d) or un conspicuous patterns (Figure 2e). The depth of the patterns was much less than those after the electrochemical reduction process. Therefore, the electrochemical process not only played a role in localized reduction, but also contributed to the imprint depth

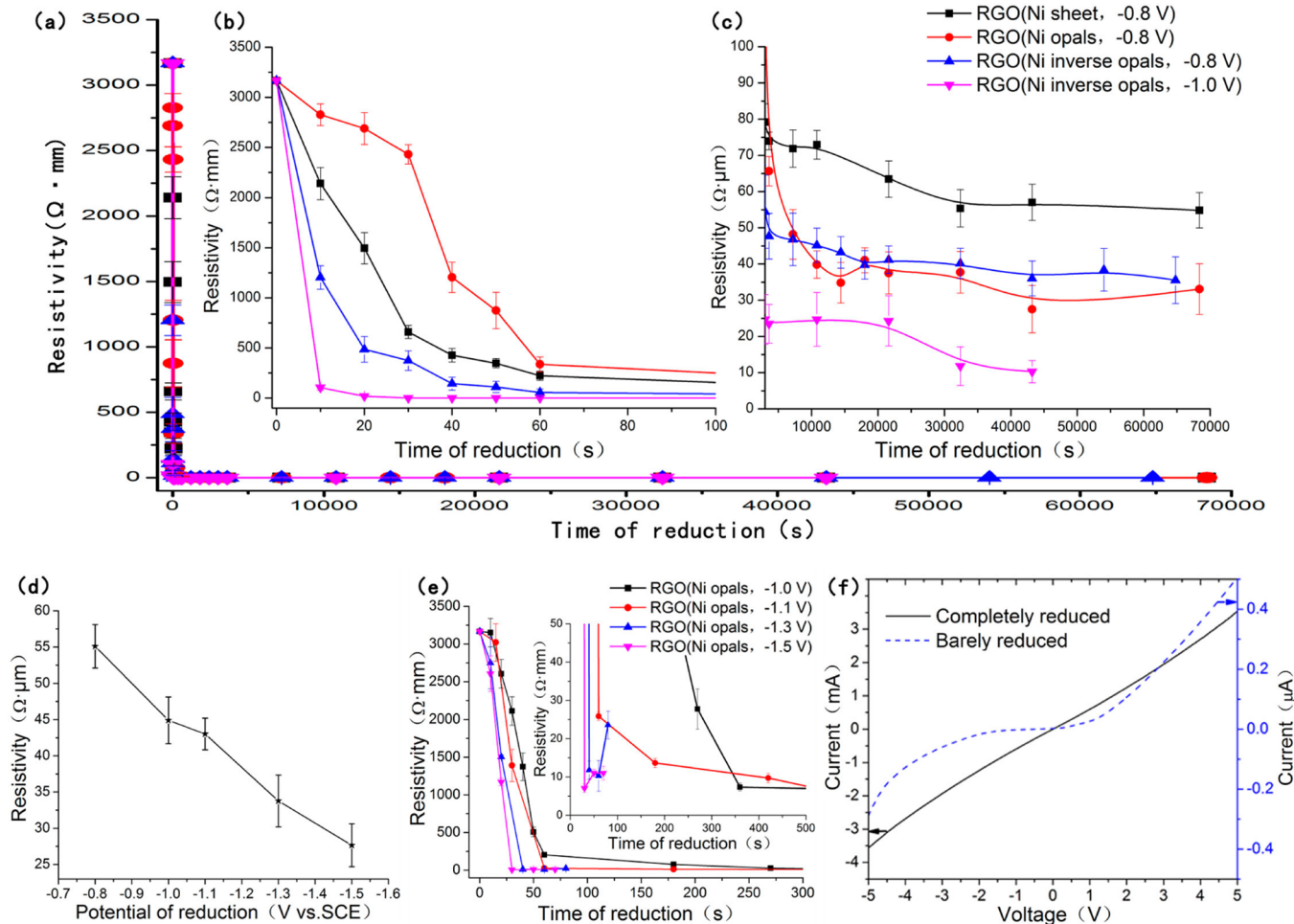


Figure 4. (a–c) Resistivity variations with the increase in the reduction time of the RGO using Ni inverse opals, opals, and solid films: (a) whole reduction period, (b) 0–100 s, and (c) 4000–70000 s. (d) Resistivity of RGO reduced at the potentials from -0.8 to -1.5 V after complete reduction. (e) Resistivity variations with the increase in the reduction time of the RGO using Ni opals. (f) Typical I – V data of RGO completely or barely reduced.

of Ni structures. This is probably because the induced water flow during the electrochemical process may help the contacting/stamping of the RGO patterns.

The 3D Ni opal structures obtained by a double replication process were also used as the patterning electrodes for GO reduction. Figure 2f,g shows the typical SEM images of fabricated ZnO inverse-opal and Ni opal structures. The resulting unreduced GO (Figure s3a) and GO with reduction times of 30 min (Figure s3b), 3 h (Figure 2h), and 9 h (Figure s3c) do not show visible imprint traces when Ni opals were used. The Ni opal structure has a much higher filling ratio compared to the inverse-opal structure. Therefore, the geometric imprint using Ni opals was relatively gentle. No visible patterns on the GO film were detected before and after the electrochemical reaction.

Figure 3a shows the typical Raman spectra of GO without reduction, RGO with different reduction times (from 10 min to 9 h) at -0.8 V using Ni inverse opals, and polystyrene colloidal crystals. The D/G intensity ratios of unreduced GO films were $\sim 1:1$. The D/G intensity ratios of all the RGO were >1 . It is understandable because the reduction of GO can produce more defects in the graphene films.^{31,42,43} Moreover, the D/G intensity ratio increased slightly with the increase in the reduction time, indicating the increase in the reduction extent.

The results are consistent with the elemental analysis by X-ray photoelectron spectroscopy (XPS) and energy dispersive X-ray spectroscopy (EDX), as shown in Figure 3b–d and Figure s4a–c. The C/O ratios of RGO films showed an increasing trend with the increase in the reduction time. More importantly, the C 1s XPS intensities of peaks belong to C in $\text{C}=\text{O}$ and $\text{C}-\text{O}$ bonds significantly decrease when the reduction time increases from 0 s (Figure 3b) to 30 s (Figure 3c) to 9 h (Figure 3d). The C 1s XPS spectra indicate the removal of the functional groups of GO though the removal is not complete at -0.8 V. No Ni or polystyrene peaks remained after removing these assisted patterning microstructures in the EDX data and Raman spectra.

The electric conductivity of the RGO samples on different Ni microstructures reduced at different potentials and reduction times were tested after coating Al electrodes on them. Figure 4a shows the overall trends of resistivity for RGO films with the increase in the reduction time under different reduction conditions (using Ni films at -0.8 V, Ni opals at -0.8 V, and Ni inverse opals at -0.8 and -1.0 V). With the increase in the reduction time, the resistivity of four RGO films showed a decreasing trend. The decrease in the resistivity during the first 200 s is very fast. Then, the decreasing speed slows down, and the resistivity of the RGO films reach the same order in

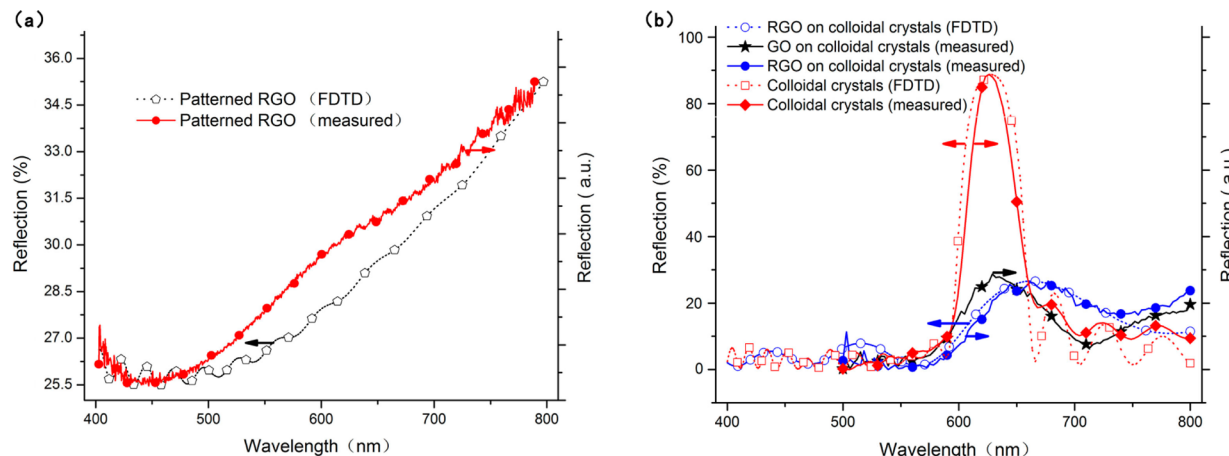


Figure 5. (a) Experimental and simulated reflection spectra of RGO with periodic undulations using Ni inverse opals. (b) Experimental and simulated reflection spectra of colloidal crystals and GO/RGO-covered colloidal crystals.

magnitude. This indicates that the reduction electrons induced exfoliations of the surface groups on GO more severely at the initial reduction, in which graphene (RGO) films were formed from GO films. The detailed changes in the resistivity of the RGO films are quite different as shown in Figure 4b when different patterning electrodes were used. The resistivity of RGO using Ni opals first changed slightly in the first 30 s and then decreased rapidly. In contrast, the resistivity of patterned GO reduced using Ni inverse opals/solid Ni films decreased rapidly at the beginning of reduction process. When the Ni opal structures were used as the patterning electrodes, the contact points between GO and Ni opals were discontinuous. The reduction electrons would spread outward centered from each contact point. As the still-disconnected nature of the RGO (Figure 1f,g), a large resistivity remained at reduction time within 30 s. As the reduction proceeded, the original disconnected RGO areas were connected to each other. Then, the resistivity decreased rapidly. In contrast, the reduction areas of RGO using the Ni inverse opals were always connected to each other at the beginning of reduction. Therefore, the resistivity of GO films decreased rapidly in the beginning of reduction. The reduction during the first 200 s, particularly below 30 s, may be important for the formation of redox patterns on graphene. All the GO would be reduced to RGO after a long reaction time. Notably, only the GO films with a 110 nm thickness were formed by chemically exfoliated GO in this study, limiting the perfect *in situ* patterning of redox status. The perfect *in situ* patterning of graphene may be produced when only one piece of GO (the oxidation state of CVD graphene) is used.

When the reduction voltage became more negative (from -0.8 to -1 V), the decrease rate of resistivity during the reduction became steeper (Figure 4b). The GO films reduced using a solid Ni film at -0.8 V had a slower reduction rate compared to that of inverse opals, as shown in the blue triangle dotted line in Figure 4b. This phenomenon indicates that the imprint of inverse-opal patterns contributed to the reduction and electric conductivity of GO films.

The special trends on the inverse opals induced reductions of GO were also confirmed by the changes in the resistivity during the reduction time in the range from 4000 to 70000 s, as shown in Figure 4c. When the RGO films were completely reduced, the resistances using Ni inverse opals or opals were slightly smaller than those using Ni solid films. This phenomenon may

be induced by the increase in the actual surface areas of RGO because of their undulated morphologies. The changes in the reduction potentials did not only affect the rate of initial reduction, but also affected the resistivity of RGO when fully reduced, as shown in the resistivity lines at -0.8 and -1 V in Figure 4c. Figure 4d shows the average resistivity after a complete reduction at the reduction potentials from -0.8 to -1.5 V using a Ni sheet. The final resistivity became smaller as the reduction potentials increased. A more complete reduction status of GO can be attributed to a high electrochemical reduction voltage.⁴⁴

Figure 4e shows the trend of the resistivity of GO films reduced using Ni opals at reduction voltages of -1.0 , -1.1 , -1.3 , and -1.5 V. The decrease rates of the resistivity were also increased with the increase in the reduction voltage. However, the changes in the resistivity (Figure 4e, inset) at reduction voltages of -1.3 and -1.5 V were not as regular as those using Ni solid films or Ni inverse opals with the increase in the reduction time. When the voltage was negative than -1.1 V, bubbles were generated near the electrodes. The RGO may detach from the patterned electrode because of the low infilling ratio of Ni opals. In that case, the patterning reduction may stop. The reduction voltage, positive than -1.1 V, is optimal in the patterning reduction process in a saturated NaCl solution though the higher voltage may lead to a more complete reduction status of GO.

Figure 4f shows two typical *I*–*V* curves for the GO/RGO films under different conditions. When GO films were reduced at -0.8 V for sufficient time (solid line in Figure 4f), a strong ohmic feature was obtained. In contrast, the *I*–*V* curve of unreduced or less reduced GO shows multijunction performance (the dashed line in Figure 4f) as several pieces of GO with different band structures may be stacked together between the two test electrodes.

The periodic undulations of RGO structures using inverse opals as the masks made them one of the promising structures for optical modulation.^{45,46} The optical performances of RGO with periodic undulations in optical wavelength were mainly studied. The measured and calculated reflection spectra of the patterned RGO structures using Ni inverse opals are shown in Figure 5a. The reflectivity of the RGO increased as the wavelength increased from 400 to 800 nm. No coupling of light was detected because of the typical dielectric dispersion⁴⁷ in optical wavelength though the periodic undulations existing in

surface geometry. The RGO films were also transferred onto the polystyrene colloidal crystals. The measured and calculated reflection spectra of colloidal crystals and RGO films covered colloidal crystals are shown in Figure Sb. The center of the reflection peak of colloidal crystals moved slightly from 626 to 635 nm when unreduced GO films were covered on colloidal crystals. The center of the reflection peak had a larger red shift (671 nm) when RGO films were covered. As a typical positive dielectric performance was exhibited by graphene in optical wavelength, the shifts in the stop band gap of colloidal crystal structures can be attributed to the interference coupling induced from RGO films.

■ CONCLUSION

The electrochemical reduction of GO using Ni inverse opals and opals as the electrodes can be successfully achieved. Several types of periodic undulations in GO can be formed according to the surface patterns of the inverse-opal structures. As shown by the reduction trends according to electric conductivity, the periodic network or disconnected dotted redox patterns of graphene can also possibly be formed at reduction time below 30 s on the surface of inverse opals or opals. The colloidal templating structure-assisted electrochemical reduction may offer a versatile approach, affording graphene with a nanoscale neck width and periodic modulations independently by controlling the size of the colloidal microspheres and reduction duration, which is different from the current 2D mask-assisted etching or photoreaction methods. The *in situ* electrochemical method shows great promise for advanced graphene electronic and photonic devices.

■ ASSOCIATED CONTENT

S Supporting Information

Typical images of Ni inverse opals showing a possible minimum contact width, GO reduced using solid Ni films, and RGO produced using Ni opals with different reduction; EDX data showing the elemental ratios of RGO. This material is available free of charge via the Internet at <http://pubs.acs.org>.

■ AUTHOR INFORMATION

Corresponding Author

*Fax: +861051688018. Tel.: +861051688018. E-mail: mfu@bjtu.edu.cn.

Notes

The authors declare no competing financial interest.

■ ACKNOWLEDGMENTS

This work was supported by National Science Foundation of China under Grant Nos. 91123025, 50902008, 61335006, and 61378013, Beijing Higher Education Young Elite Teacher Project No. YETP0574, and the National Basic Research Program of China Nos. 2011CB932700 and 2011CB932703.

■ REFERENCES

- (1) Bae, S.; et al. Roll-to-Roll Production of 30-Inch Graphene Films for Transparent Electrodes. *Nat. Nanotechnol.* **2010**, *5*, 574–8.
- (2) Novoselov, K. S.; Fal, V.; Colombo, L.; Gellert, P.; Schwab, M.; Kim, K. A Roadmap for Graphene. *Nature* **2012**, *490*, 192–200.
- (3) Han, T. H.; Lee, Y.; Choi, M. R.; Woo, S. H.; Bae, S. H.; Hong, B. H.; Ahn, J. H.; Lee, T. W. Extremely Efficient Flexible Organic Light-Emitting Diodes with Modified Graphene Anode. *Nat. Photonics* **2012**, *6*, 105–110.
- (4) Lin, Y. M.; Dimitrakopoulos, C.; Jenkins, K. A.; Farmer, D. B.; Chiu, H. Y.; Grill, A.; Avouris, P. 100-Ghz Transistors from Wafer-Scale Epitaxial Graphene. *Science* **2010**, *327*, 662–662.
- (5) Sun, Z.; Hasan, T.; Torrisi, F.; Popa, D.; Privitera, G.; Wang, F.; Bonaccorso, F.; Basko, D. M.; Ferrari, A. C. Graphene Mode-Locked Ultrafast Laser. *ACS Nano* **2010**, *4*, 803–810.
- (6) Mueller, T.; Xia, F.; Avouris, P. Graphene Photodetectors for High-Speed Optical Communications. *Nat. Photonics* **2010**, *4*, 297–301.
- (7) Bao, Q.; Zhang, H.; Wang, B.; Ni, Z.; Lim, C. H. Y. X.; Wang, Y.; Tang, D. Y.; Loh, K. P. Broadband Graphene Polarizer. *Nat. Photonics* **2011**, *5*, 411–415.
- (8) Liu, M.; Yin, X.; Ulin-Avila, E.; Geng, B.; Zentgraf, T.; Ju, L.; Wang, F.; Zhang, X. A Graphene-Based Broadband Optical Modulator. *Nature* **2011**, *474*, 64–67.
- (9) Yang, J.; Gunasekaran, S. Electrochemically Reduced Graphene Oxide Sheets for Use in High Performance Supercapacitors. *Carbon* **2013**, *51*, 36–44.
- (10) Lian, P.; Zhu, X.; Liang, S.; Li, Z.; Yang, W.; Wang, H. Large Reversible Capacity of High Quality Graphene Sheets as an Anode Material for Lithium-Ion Batteries. *Electrochim. Acta* **2010**, *55*, 3909–3914.
- (11) Geim, A. K. Graphene: Status and Prospects. *Science* **2009**, *324*, 1530–1534.
- (12) Wang, X.; Zhi, L.; Müllen, K. Transparent, Conductive Graphene Electrodes for Dye-Sensitized Solar Cells. *Nano Lett.* **2008**, *8*, 323–327.
- (13) Li, X.; Zhu, Y.; Cai, W.; Borysiak, M.; Han, B.; Chen, D.; Piner, R. D.; Colombo, L.; Ruoff, R. S. Transfer of Large-Area Graphene Films for High-Performance Transparent Conductive Electrodes. *Nano Lett.* **2009**, *9*, 4359–4363.
- (14) Wang, Y.; Shao, Y.; Matson, D. W.; Li, J.; Lin, Y. Nitrogen-Doped Graphene and Its Application in Electrochemical Biosensing. *ACS Nano* **2010**, *4*, 1790–1798.
- (15) Castro, E. V.; Novoselov, K.; Morozov, S.; Peres, N.; Dos Santos, J. L.; Nilsson, J.; Guinea, F.; Geim, A.; Neto, A. C. Biased Bilayer Graphene: Semiconductor with a Gap Tunable by the Electric Field Effect. *Phys. Rev. Lett.* **2007**, *99*, 216802.
- (16) Mikhailov, S. Theory of the Giant Plasmon-Enhanced Second-Harmonic Generation in Graphene and Semiconductor Two-Dimensional Electron Systems. *Phys. Rev. B* **2011**, *84*, 045432.
- (17) Da, H.; Qiu, C.-W. Graphene-Based Photonic Crystal to Steer Giant Faraday Rotation. *Appl. Phys. Lett.* **2012**, *100*, 241106.
- (18) Berger, C.; Song, Z.; Li, X.; Wu, X.; Brown, N.; Naud, C.; Mayou, D.; Li, T.; Hass, J.; Marchenkov, A. N. Electronic Confinement and Coherence in Patterned Epitaxial Graphene. *Science* **2006**, *312*, 1191–1196.
- (19) Wang, X.; Ouyang, Y.; Jiao, L.; Wang, H.; Xie, L.; Wu, J.; Guo, J.; Dai, H. Graphene Nanoribbons with Smooth Edges Behave as Quantum Wires. *Nat. Nanotechnol.* **2011**, *6*, 563–567.
- (20) Liu, L.; Zhang, Y.; Wang, W.; Gu, C.; Bai, X.; Wang, E. Nanosphere Lithography for the Fabrication of Ultrnarow Graphene Nanoribbons and on-Chip Bandgap Tuning of Graphene. *Adv. Mater.* **2011**, *23*, 1246–1251.
- (21) Weitz, R. T.; Allen, M.; Feldman, B.; Martin, J.; Yacoby, A. Broken-Symmetry States in Doubly Gated Suspended Bilayer Graphene. *Science* **2010**, *330*, 812–816.
- (22) Son, Y.-W.; Cohen, M. L.; Louie, S. G. Energy Gaps in Graphene Nanoribbons. *Phys. Rev. Lett.* **2006**, *97*, 216803.
- (23) Chen, Z.; Lin, Y.-M.; Rooks, M. J.; Avouris, P. Graphene Nano-Ribbon Electronics. *Physica E* **2007**, *40*, 228–232.
- (24) Ponomarenko, L.; Schedin, F.; Katsnelson, M.; Yang, R.; Hill, E.; Novoselov, K.; Geim, A. Chaotic Dirac Billiard in Graphene Quantum Dots. *Science* **2008**, *320*, 356–358.
- (25) Zhang, L.; Diao, S.; Nie, Y.; Yan, K.; Liu, N.; Dai, B.; Xie, Q.; Reina, A.; Kong, J.; Liu, Z. Photocatalytic Patterning and Modification of Graphene. *J. Am. Chem. Soc.* **2011**, *133*, 2706–2713.
- (26) Akhavan, O. Graphene Nanomesh by Zno Nanorod Photocatalysts. *ACS Nano* **2010**, *4*, 4174–4180.

- (27) Shi, Z.; Yang, R.; Zhang, L.; Wang, Y.; Liu, D.; Shi, D.; Wang, E.; Zhang, G. Patterning Graphene with Zigzag Edges by Self-Aligned Anisotropic Etching. *Adv. Mater.* **2011**, *23*, 3061–3065.
- (28) Safron, N. S.; Brewer, A. S.; Arnold, M. S. Semiconducting Two-Dimensional Graphene Nanoconstriction Arrays. *Small* **2011**, *7*, 492–498.
- (29) Bai, J.; Zhong, X.; Jiang, S.; Huang, Y.; Duan, X. Graphene Nanomesh. *Nat. Nanotechnol.* **2010**, *5*, 190–194.
- (30) Kim, T. Y.; Kwon, S. W.; Park, S. J.; Yoon, D. H.; Suh, K. S.; Yang, W. S. Self-Organized Graphene Patterns. *Adv. Mater.* **2011**, *23*, 2734–2738.
- (31) Sinitskii, A.; Tour, J. M. Patterning Graphene through the Self-Assembled Templates: Toward Periodic Two-Dimensional Graphene Nanostructures with Semiconductor Properties. *J. Am. Chem. Soc.* **2010**, *132*, 14730–14732.
- (32) Zhou, Y.; Bao, Q.; Varghese, B.; Tang, L. A. L.; Tan, C. K.; Sow, C. H.; Loh, K. P. Microstructuring of Graphene Oxide Nanosheets Using Direct Laser Writing. *Adv. Mater.* **2010**, *22*, 67–71.
- (33) Ramesha, G. K.; Sampath, S. Electrochemical Reduction of Oriented Graphene Oxide Films: An In Situ Raman Spectroelectrochemical Study. *J. Phys. Chem. C* **2009**, *113*, 7985–7989.
- (34) Pei, S.; Cheng, H.-M. The Reduction of Graphene Oxide. *Carbon* **2012**, *50*, 3210–3228.
- (35) Low, C.; Walsh, F.; Chakrabarti, M.; Hashim, M.; Hussain, M. Electrochemical Approaches to the Production of Graphene Flakes and Their Potential Applications. *Carbon* **2013**, *54*, 1–21.
- (36) Wang, Z.; Zhou, X.; Zhang, J.; Boey, F.; Zhang, H. Direct Electrochemical Reduction of Single-Layer Graphene Oxide and Subsequent Functionalization with Glucose Oxidase. *J. Phys. Chem. C* **2009**, *113*, 14071–14075.
- (37) Shao, Y.; Wang, J.; Engelhard, M.; Wang, C.; Lin, Y. Facile and Controllable Electrochemical Reduction of Graphene Oxide and Its Applications. *J. Mater. Chem.* **2010**, *20*, 743–748.
- (38) Ekiz, O. O.; Urel, M.; Guner, H.; Mizrak, A. K.; Dâna, A. Reversible Electrical Reduction and Oxidation of Graphene Oxide. *ACS Nano* **2011**, *5*, 2475–2482.
- (39) Guo, H. L.; Wang, X. F.; Qian, Q. Y.; Wang, F. B.; Xia, X. H. A Green Approach to the Synthesis of Graphene Nanosheets. *ACS Nano* **2009**, *3*, 2653–2659.
- (40) David, L.; Bhandavat, R.; Kulkarni, G.; Pahwa, S.; Zhong, Z.; Singh, G. Synthesis of Graphene Films by Rapid Heating and Quenching at Ambient Pressures and Their Electrochemical Characterization. *ACS Appl. Mater. Interfaces* **2013**, *5*, 546–552.
- (41) Xu, X.; Huang, D.; Cao, K.; Wang, M.; Zakeeruddin, S. M.; Graetzel, M. Electrochemically Reduced Graphene Oxide Multilayer Films as Efficient Counter Electrode for Dye-Sensitized Solar Cells. *Sci. Rep.* **2013**, *3*.
- (42) Zhu, Y.; Murali, S.; Cai, W.; Li, X.; Suk, J. W.; Potts, J. R.; Ruoff, R. S. Graphene and Graphene Oxide: Synthesis, Properties, and Applications. *Adv. Mater.* **2010**, *22*, 3906–3924.
- (43) Ferrari, A.; Meyer, J.; Scardaci, V.; Casiraghi, C.; Lazzeri, M.; Mauri, F.; Piscanec, S.; Jiang, D.; Novoselov, K.; Roth, S. Raman Spectrum of Graphene and Graphene Layers. *Phys. Rev. Lett.* **2006**, *97*, 187401.
- (44) Zeng, Y.; Zhou, Y.; Kong, L.; Zhou, T.; Shi, G. A Novel Composite of SiO₂-Coated Graphene Oxide and Molecularly Imprinted Polymers for Electrochemical Sensing Dopamine. *Biosens. Bioelectron.* **2013**, *45*, 25–33.
- (45) Yan, H.; Li, X.; Chandra, B.; Tulevski, G.; Wu, Y.; Freitag, M.; Zhu, W.; Avouris, P.; Xia, F. Tunable Infrared Plasmonic Devices Using Graphene/Insulator Stacks. *Nat. Nanotechnol.* **2012**, *7*, 330–334.
- (46) Grigorenko, A.; Polini, M.; Novoselov, K. Graphene Plasmonics. *Nat. Photonics* **2012**, *6*, 749–758.
- (47) Palik, E. D. *Handbook of Optical Constants of Solids*; Academic Press: New York, 1998; Vol. 3.